AIP | Applied Physics Letters

Selective absorption and emission on magnetic transitions in low dimensional dielectric structures

Roman Shugayev and Peter Bermel

Citation: Applied Physics Letters **108**, 071106 (2016); doi: 10.1063/1.4942392
View online: http://dx.doi.org/10.1063/1.4942392
View Table of Contents: http://scitation.aip.org/content/aip/journal/apl/108/7?ver=pdfcov
Published by the AIP Publishing

Selective absorption and emission on magnetic transitions in low dimensional dielectric structures

Roman Shugayev and Peter Bermel[a)]
Purdue Quantum Center and Birck Nanotechnology Center, 1205 W. State St, Purdue University, West Lafayette, Indiana 47907, USA

(Received 26 November 2015; accepted 6 February 2016; published online 18 February 2016)

Solid-state systems have potential advantages as platforms for manipulating spin states in several applications, such as quantum computing. Here, it is most desirable to utilize the zero phonon line (ZPL), since its corresponding states are partially shielded from loss and dephasing, but it often directly overlaps in frequency with broadened phonon sidebands at room temperature. The ZPL in solid-state spin systems, such as xenon vacancy centers in diamond and transition metal ions in crystals, is often magnetic dipole (MD), whereas the broadened phonon sideband is predominantly electric dipole (ED). In this letter, we numerically demonstrate a nanorod system that efficiently suppresses ED absorption, and furthermore allows selective detection of emitted radiation originating from MD transitions. The factor of suppression of electric absorption is 1.3×10^4, while the factor of detected ED emission suppression is 20 in the plane. We also show that a nanoparticle suppresses ED emission by a factor of 12. This approach can allow nanoscale decoupling of ZPL from the phonon sidebands, thus facilitating the use of solid-state material systems with MD ZPL transitions for on-chip quantum applications. © *2016 AIP Publishing LLC*.
[http://dx.doi.org/10.1063/1.4942392]

Strong interaction with states shielded from dephasing and nonradiative losses through the zero phonon line (ZPL) are necessary to maintain coherence, in particular, for both the generation of remotely entangled multi-qubit photon states and creation of single photon sources.[1,2] For these reasons, interactions through ZPL transitions have recently been studied.[3–5] Separate research on transition metal ions has shown that ZPLs from Mg^{4+}, V^{2+}, and Cr^{3+} in crystalline hosts, such as MgO, can be magnetic in nature, while the overlapping phonon emission has a highly electric dipole character.[6–8] With a properly designed quantum state and local emitter environment, one could selectively address such magnetic ZPL transitions in various systems, and reduce the detrimental effect of phonon broadening at elevated temperatures.

MD emission and absorption have received significant research attention in the past several years. Several material systems such as lanthanide ions and transitional metals have been investigated.[8–10] Structures like metal mirrors, nanolayers, and plasmonic nanostrip arrays have been proposed for selective far field emission originating from MD transitions.[8–11] Selective excitation of MD transitions has also been demonstrated using azimuthally polarized beams.[12]

In this paper, we demonstrate that a doped nanocrystal embedded in the cylindrical nanorod having a high refractive index permits a sharp distinction between MD and ED transitions. High electric dipole absorption suppression is achieved by placing the structure in the bull's eye of azimuthally polarized beam. Emission of two electric dipole polarizations (E_x and E_y) are suppressed due to the high index contrast reflection of the nanorod walls, while the third polarization (E_z) is canceled using a polarizer. As an example of an experimental system, we show that by embedding a Cr^{3+}-doped MgO nanocrystal in a silicon nanorod, the 698 nm ZPL $^2E \rightarrow {}^4A_2$ transition can be accessed and read, while strongly suppressing spurious interactions.

Azimuthally polarized beams can be generated using several techniques, such as liquid crystal polarization converters, diffractive interferometers, or fiber-optic solutions.[13–15] In this work, we have analyzed excitation through azimuthally polarized beam for the case of the nanorod positioned in the bull's eye of the beam at the beam waist, with the nanorod axis coinciding with the beam axis [Fig. 1(a)].

The electric field for the azimuthally polarized Laguerre–Gaussian $p = 0$ and $l = 1$ mode are given by[16]

$$\mathrm{E}(r,\theta) = \hat{\theta} E_0 \sqrt{2} \frac{r}{w_0} \exp\left(-\frac{r^2}{w_0^2}\right) \exp(i\theta) \exp(ik_h z). \quad (1)$$

We approximate the corresponding magnetic field at $r/w_0 \ll 1$ by

$$\mathrm{H}(r,\theta) = \hat{z} i E_0 \sqrt{2} \frac{\lambda}{Z\pi w_0} \exp\left(-\frac{r^2}{w_0^2}\right) \exp(i\theta) \exp(ik_h z), \quad (2)$$

where Z is the impedance of the medium, λ is the wavelength in the medium, w_o is the beam waist, and k_h is the wavevector in the z-direction. It is clear from the field distribution that magnetic field has a smooth Gaussian shape, with a maximum at the center of the beam while electric field approaches zero linearly with distance to the center. The absorption rate $W = fNI$, where f is the oscillator strength, N is the ion concentration, and I is the field intensity. The field intensity in terms of electric and magnetic fields is

a)Author to whom correspondence should be addressed. Electronic mail: pbermel@purdue.edu.

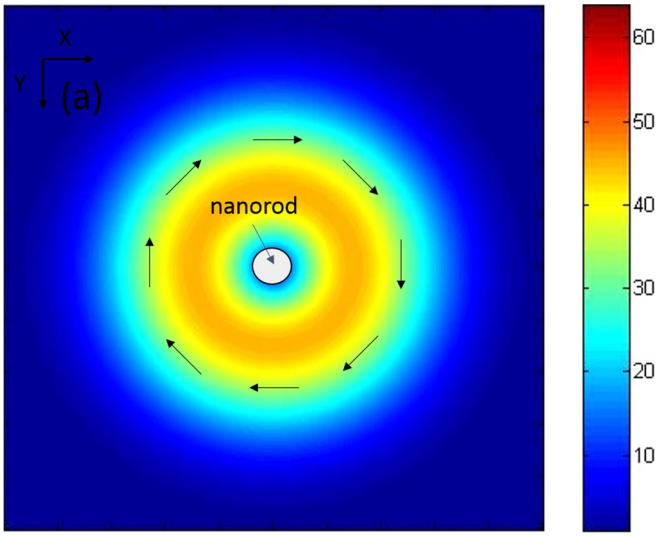

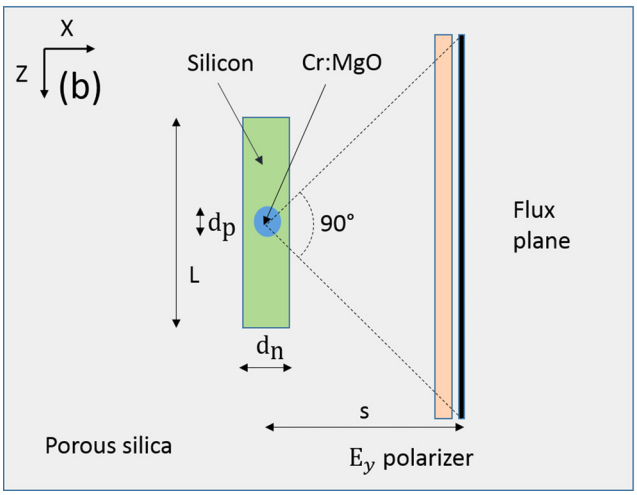

FIG. 1. (a) Electric field amplitude of an azimuthally polarized beam. The nanorod structure (shown in white) is positioned in the bull's eye of the beam. Black arrows specify direction of electric field. (b) A layout of the detection scheme for the MD and ED polarized emissions, along with its characteristic geometric parameters.

given by $I = \varepsilon_h \nu |E|^2/2$ and $I = \varepsilon_h \nu Z^2 |H|^2/2$, respectively, where v is the speed of light in the medium and ε_h is the host permittivity.

We simulated emission from the nanorod structure in 3 dimensions, as shown in Fig. 1(b), using a freely available electromagnetic simulation package known as MEEP[17] on the Purdue Carter community computer cluster.[18] For high accuracy, the grid spacing for the 3D simulations was set as 0.3 nm. Magnetic and electric unit dipole sources were placed at the center of the nanocrystal and were assumed to emit isotropically. The average emitted power was then computed by time-averaging the Poynting vector component in the x direction after passing through an ideal polarizer with an Ey transmission axis. The only non-zero contribution is $E_y(t) \cdot H_z(t)$, because the $E_z(t) \cdot H_y(t)$ term vanishes when E_z is screened out. As discussed later, the nanorod orientation itself may be able to substitute for the polarizer. The flux in the x-direction, spanning a $2\pi/3$ steradian solid angle, was then analyzed. Emission fluxes were computed both in the far field and in the near field, and were shown to produce the same results therefore for high-resolution 3D simulations near field fluxes were used to minimize the computational load. All flux planes in subsequent analysis was located at a distance $s = L$ from the center of the nanocrystal and had dimensions of $2L \times 2L$. For Cr^{3+}:MgO and silicon, the refractive indices were taken to be $n_p = 1.73 + 0.00023i$ and $n_r = 3.78 + 0.0026i$ at 698 nm, respectively.[19,20] To maximize the refractive index contrast between the nanorod and the medium host material, the latter was assumed to be low-k porous silica, with a refractive index of $n = 1.1$.[21]

To efficiently absorb the energy via ZPL selective excitations of MD transition, it is necessary to reduce spurious nanorod absorption. The ratio between the electric and magnetic field magnitudes in the center of the focused beam described by Eqs. (1) and (2) can be approximated as $|H(r,\theta)|/|E(r,\theta)| = \lambda/(Z\pi r)$. We can view this problem through the quasistatic approximation. In the case of the central region of the azimuthally polarized beam, $\int B \cdot H dV / \int D \cdot E dV \gg 1$ and $r \ll \lambda$. Therefore, the magnetostatic approximation can be employed. This implies that electric fields are set through Faraday's law with magnetic fields acting as a source and, due to purely transverse boundary condition, both the electric and magnetic fields in the bull's eye region are only perturbed from the homogeneous case by a change in the effective medium permittivity. In this case, $r_0/\lambda = 0.004$, where r_0 is the nanorod radius, and thus, the perturbation can be neglected for our analysis. Therefore, we can directly use local fields for the homogeneous medium defined in Equations (1) and (2) to estimate the ratio of Cr^{3+} ZPL absorbed power to spuriously absorbed power.

The Cr^{3+}:MgO absorption was estimated from experimental data[19] to be $\alpha = 8\ cm^{-1}$ at 10% doping levels for the media with effective refractive index $n = 1.1$. The silicon absorption coefficient is taken to be $\alpha = 440\ cm^{-1}$ (at 698 nm).[20] Absorption ratio of ED and MD transitions using data from Ref. 22 was assumed to be 5:1. Ratio of ED and MD absorption as well as spurious absorption was derived from the absorption rate equations above, using local electric and magnetic fields. The setup was optimized over a range of nanorod diameter and lengths, as well as beam diameter values attainable at this wavelength. We found that smaller beam diameters generally yield higher ratio of absorbed to total power, while the nanorod gives lowest spurious absorption for the smallest diameter values (preferably, 5 nm or below). The height of the nanorod was selected to provide high suppression factor which tends to plateau for $L/d_n > 5$. Based on this work, the nanorod diameter and height were set to $d_n = 5$ nm and $L = 25$ nm, respectively, while the diameter of the Cr^{3+}:MgO spherical nanocrystal was set to a value $d_p = 3.75$ nm. In this geometry, the suppression of the electric dipole absorption due to the azimuthal beam excitation, compared to the vacuum plane wave excitation case, was calculated to be a factor of 1.3×10^4, despite the typical enhancement associated with presence in a higher index medium.

Given the above parameters, and taking into account the nonuniform electric field distribution within the nanorod, we obtain the power absorbed by ZPL magnetic transition to be 94% of the total absorbed power. The portion of radiation

absorbed by the ED transitions in the Cr^{3+}:MgO nanocrystal at $\lambda = 698\,\text{nm}$ is 0.032%. By comparison, a nanocrystal within nanorod excited by a plane-wave would only yield 4% of the total absorption as a ZPL magnetic transition. The ratio of absorbed to total power carried by the azimuthally polarized beam is 5.33×10^{-13}, assuming $w_0 = \lambda$. Total power was calculated by integrating the $E_\theta \times H_r$ Poynting vector in the XY plane. Average power absorbed via magnetic transition was computed using $P^m_{abs} = \omega\mu''|H|^2 V/2$,[22] where μ' is imaginary part of magnetic permeability, and V is the nanocrystal volume.

The Laguerre-Gaussian modes with $l > 0$ carry angular momentum, and therefore may suppress scattering, due to the elimination of the lowest-order spherical harmonic scattering mode. In particular, angular-momentum-induced transparency has been suggested for the nanoparticles in Ref. 23. Following the same procedure, we calculated the ratio of scattered to absorbed power for the $a = 2.5\,\text{nm}$ radius silicon particle for the Laguerre-Gaussian $p = 0$, $l = 1$ mode will be 2×10^{-15}. For a plane wave excitation, the same factor would be 3.9, as calculated using Rayleigh total power scattering formula

$$P_s = \frac{4\pi}{3Z} k^4 a^6 \left(\frac{\varepsilon_p - \varepsilon_h}{\varepsilon_p + 2\varepsilon_h}\right)^2 |E_0|^2, \tag{3}$$

where ε_p is a particle permittivity. Therefore, azimuthal excitation presents significant advantage from the scattering perspective, especially for low absorbing materials. This effect should similarly hold for the analyzed nanorod structure, due to the same excitation mode profile and azimuthal boundary conditions.

Emission suppression due to subwavelength dielectric confinement in thin layers has been investigated previously.[24] In particular, it has been shown that $P_e^{\perp} = P_e^{0,\perp}(\varepsilon_h/\varepsilon_l)^2$ and $P_m^{\parallel} = P_m^{0,\parallel}$, where $P_e^{\perp}$, $P_m^{\parallel}$ and $P_e^{0,\perp}$, $P_m^{0,\parallel}$ are powers emitted by the out-of-plane polarized electric dipole and in-plane polarized magnetic dipoles in the thin layer and in the host material, respectively, and ε_l is the permittivity of the thin layer. We verified that this scaling with a thin dielectric layer finite-difference time domain (FDTD) simulations. In particular, we found that for silicon/porous silica system out-of-plane polarized electric dipole emission rate is reduced by a factor of 141 relative to the host material. Intuitively, from the point of view of the Poynting theorem, the electric dipole suppression can be seen as a result of the out-of-phase reflected E field suppressing the $J \cdot E$ input power term. The out-of-phase reflections take place due to boundary conditions, which cannot support propagating modes along the plane of the thin layer.

From this previous work, it is clear that increasing the spatial confinement through thin sheets, as well as the contrast between the permittivities of the host and the thin layer, can both insure a high level of electric dipole emission suppression. However, this effect only extends over a very narrow range of angles. As a result, the total suppression of the detectable radiated power is small, because emission at other angles is not suppressed. Thus, to make practical use of this phenomenon, it is important to extend this effect over a broader angular range.

Reducing the dimensionality of the structure to a nanorod with a small radius creates 2D spatial confinement, which allows it to separate magnetic dipole emission from electric dipole emission over this broader range of angles. The trade-off associated with increased confinement is lowering of the maximum suppression factor, due to reduced out-of-phase reflections. For a Cr^{3+}: MgO nanocrystal embedded in a silicon nanorod with the geometry given above, we obtained a factor of 20 suppression of electric dipole emission, along with the associated magnetic dipole emission losses of <1%. It is to a large degree insensitive to exact position of the nanocrystal within nanorod, shown in Fig. 2(b), with a relative change of about 3% for a 6 nm shift in position of the particle (assuming it stays within the nanorod). Furthermore, the suppression effect extends over broad range of subwavelength nanorod dimensions, as shown in Fig. 3. For larger structures, there is also an increase in emission rate due to the higher density of states. This increased emission rate comes at the price not only of a larger form factor but also increased spurious absorption. The overall emission of the ED radiation for this geometry is reduced by 57%, which should improve the dephasing dynamics of the quantum state.

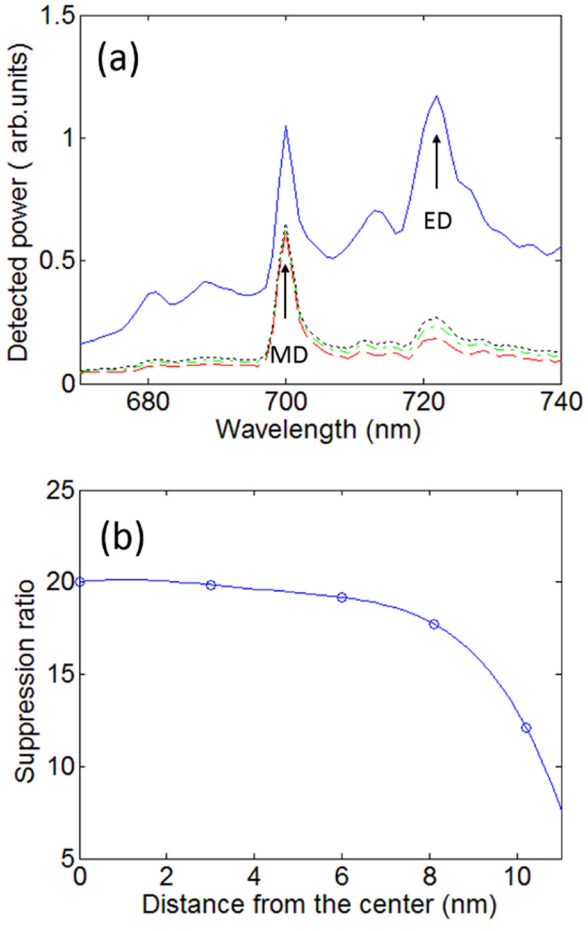

FIG. 2. (a) Total detected power without the structure (blue solid), with the nanorod structure (green dashed dot), nanoparticle structure (black dot) and emitted via magnetic dipole (MD)-only transitions (red dash). The spectral profile produced using data from Ref. 8. Electric dipole (ED) and MD transitions are depicted. (b) Suppression ratio versus position of the nanocrystal along z direction from the center of the nanorod.

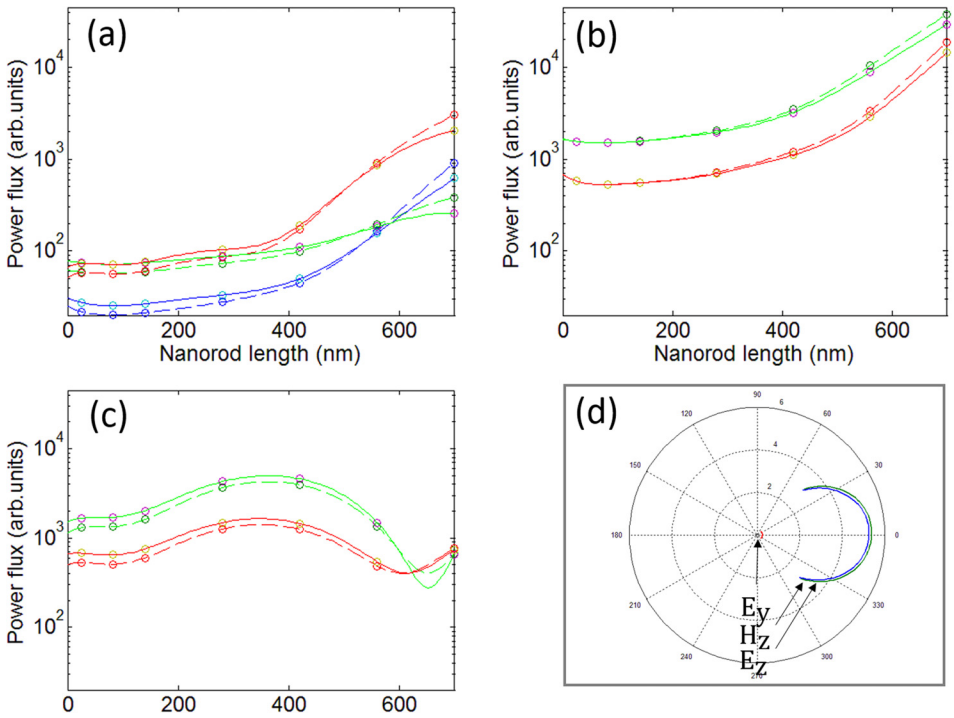

FIG. 3. Power flux versus nanorod size in Y (blue), X (green), and Z (red) direction for (a) E_y, (b) H_z, and (c) E_z dipoles in MgO nanocrystal (solid) and diamond nanocrystal (dashed). Note that all structure dimensions are scaled maintaining the same aspect ratio. (d) Polar plot showing XZ plane distribution of emitted flux for H_z (blue), E_z (green), and E_y (red) dipoles for 25 nm long nanorod. The results are calculated without a polarizer.

Alternatively, a silicon coated MgO nanoparticle instead of the nanorod may be used. The advantages of using this geometry include isotropic suppression of electric dipole emissions and reduced host absorption losses. The estimated absorbed ZPL power is 97%. The electric emission suppression factor is lower than for the nanorod (a factor of 12 for 5 nm diameter silicon, with a 2.5 nm diameter embedded crystal), again due to reduced out-of-phase reflections. However, since it is isotropic, the overall ED emission will be significantly lower, reduced by about 92%. Fig. 2(a) shows estimated emission spectrum at the room temperature for Cr^{3+}:MgO nanocrystal embedded into nanorod structure and nanoparticle structure.

Importantly, the high index embedded methodology presented here is very generic, and to a large degree insensitive to the refractive index of the embedded nanocrystal. Thus, other crystalline materials with suitable dopants shielded from high dephasing rates may be utilized in a similar manner to facilitate access to magnetic ZPL transitions. For instance, it has previously been shown that a xenon impurity ZPL in diamond also has a magnetic dipole nature.[25] Figure 3 shows emission plots versus the size of the nanorod for diamond nanocrystals.

In this work, we have chosen the dimensions of the analyzed structure to reduce spurious absorption by utilizing the null electric field at the bull's eye of the azimuthal beam. The linear absorption of silicon at 698 nm is the main physical mechanism for such energy loss. Operating on the magnetic transition lines below the bandgap of the high refractive index material, or in the applications where high absorption efficiency is not required will permit the use of structures with larger dimensions. This approach can also permit the use of materials with higher index of refraction, such as germanium, since the scaling for the thin film goes as the fourth power of the refractive index contrast between the thin layer and the host material.

Very small dimensions can readily be achieved using the nanorod structure approach; this would be beneficial for design of nanoscale arrays and quantum networks coupled through far field emissions[2] and/or nearest neighbor spin interactions[26] which extend over a limited range on the order of 20–30 nm. Such arrays would have intrinsic polarizer properties, due to substantial differences in absorption for each polarization, which would greatly reduce spurious interactions and potentially eliminate the need for external polarizers, which could in turn reduce losses. Indeed, internal fields are reduced substantially for high refractive index cylinder with permittivity ε_r in the quasistatic E_x field $E_x^{int} = \frac{2\varepsilon_h}{\varepsilon_h+\varepsilon_r} E_x^0$. Using FDTD simulations, we obtained the ratio of absorption coefficients between polarizations normal and parallel to the nanorod axis for the silicon/porous silica nanorod system with dimensions given above is 22. Furthermore, suppression of electric dipole emission that could couple H_z-oriented dipoles in the neighboring nanorods (assuming XY plane positioned z-oriented nanorods) should minimize spurious interactions between nanorods, ultimately increasing coherent lifetimes. Azimuthal bull's eye excitation, potentially augmented by a field-induced resonance shift, can allow selective addressing of individual nanocrystals at nanoscale spacing, thus permitting further miniaturization for potential on-chip applications. Alternatively, we can also envision systems where individual nanocrystals are deterministically positioned and nearest-neighbor coupled inside single nanorod along the nanorod axis for the creation of quantum registers.

Future work should focus on the fabrication and characterization of the nanorod devices described above operating on magnetic dipole transitions. The porous silica matrix could be fabricated using sol-gel techniques for low-k material fabrication.[19] Embedding very small nanoparticles in the mesoporous silica matrices has been reported in the literature.[27] Alternatively, a prefabricated structure could also be suspended in air using optical trapping techniques, which

would also improve suppression ratio due to lowering of the host medium refractive index. Nanorod structures can be produced using e-beam lithography with feature sizes as small as 6 nm.[28] Both spherical and cubic geometries for MgO nanocrystals have been shown in the in the experiment.[29] However, no work to date that we know of has reported placing these nanocrystals within the nanorods.

Selective control of MD transitions presents a paradigm for realization of nanoscale quantum optical devices. Having the ability to read-out and access magnetic transitions, while suppressing electric emission—even at room temperature—may result in optical devices operating with high performance in previously unusable material systems.

[1]H. Bernien, B. Hensen, W. Pfaff, G. Koolstra, M. S. Blok, L. Robledo, T. H. Taminiau, M. Markham, D. J. Twitchen, L. Childress, and R. Hanson, Nature **497**, 86 (2013).
[2]L. J. Rogers, K. D. Jahnke, T. Teraji, L. Marseglia, C. Müller, B. Naydenov, H. Schauffet, C. Kranz, J. Isoya, L. P. McGuiness, and F. Jelezko, Nat. Commun. **5**, 4739 (2014).
[3]J. Hansom, C. H. Schulte, C. Matthiesen, M. J. Stanley, and M. Atatüre, Appl. Phys. Lett. **105**, 172107 (2014).
[4]J. Wolters, A. W. Schell, G. Kewes, N. Nüsse, M. Schoengen, H. Döscher, T. Hannappel, B. Löchel, M. Barth, and O. Benson, Appl. Phys. Lett. **97**, 141108 (2010).
[5]Q. Liu, Z. Ouyang, and S. Albin, Opt. Laser Technol. **48**, 128 (2013).
[6]G. F. Imbusch, W. M. Yen, A. L. Schawlow, D. E. McCumber, and M. D. Sturge, Phys. Rev. **133**, 1029 (1964).
[7]B. Henderson and T. P. P. Hall, Proc. Phys. Soc. **90**, 511 (1967).
[8]S. Karaveli, S. Wang, G. Xiao, and R. Zia, ACS Nano **7**, 7165 (2013).
[9]S. Karaveli and R. Zia, Phys. Rev. Lett. **106**, 193004 (2011).
[10]T. H. Taminiau, S. Karaveli, N. F. van Hulst, and R. Zia, Nat. Commun. **3**, 979 (2012).
[11]N. Noginova, R. Hussain, M. A. Noginov, J. Vella, and A. Urbas, Opt. Express **21**, 23087 (2013).
[12]M. Kasperczyk, S. Person, D. Ananias, L. D. Carlos, and L. Novotny, Phys. Rev. Lett. **114**, 163903 (2015).
[13]M. Stalder and M. Schadt, Opt. Lett. **21**, 1948 (1996).
[14]K. C. Toussaint, S. Park, J. E. Jureller, and N. F. Scherer, Opt. Lett. **30**, 2846 (2005).
[15]R. Zheng, C. Gu, A. Wang, L. Xu, and H. Ming, Opt. Express **18**, 10834 (2010).
[16]R. Oron, S. Blit, N. Davidson, A. A. Friesem, Z. Bomzon, and E. Hasman, Appl. Phys. Lett. **77**, 3322 (2000).
[17]A. F. Oskooi, D. Roundy, M. Ibanescu, P. Bermel, J. D. Joannopoulos, and S. G. Johnson, Comput. Phys. Commun. **181**, 687 (2010).
[18]See http://www.rcac.purdue.edu/userinfo/resources/carter/ for "Rosen Center for Advanced Computing: Carter User Information" (last accessed on October 20, 2015).
[19]S. Kuck, L. Fornasiero, E. Heumann, E. Mix, G. Huber, T. Karner, and A. Maaroos, Laser Phys. Lawrence **10**, 411 (2000), available at http://www.maik.ru/full/lasphys_archive/00/2/lasphys2_00p411full.pdf.
[20]G. Vuye, S. Fisson, V. Nguyen Van, Y. Wang, J. Rivory, and F. Abeles, Thin Solid Films **233**, 166 (1993).
[21]Y. Zhang, C. Zhao, P. Wang, L. Ye, J. Luo, and B. Jiang, Chem. Commun. **50**, 13813 (2014).
[22]M. K. Krage, Am. Ceram. Soc. Bull. **60**, 1232 (1981).
[23]A. S. Rury and R. Freeling, Phys. Rev. A **86**, 053830 (2012).
[24]W. Lukosz, J. Opt. Soc. Am. **71.6**, 744 (1981).
[25]Y. Dziashko, "Optical spectroscopy of xenon-related defects in diamond," *All Dissertations, Theses, and Capstone Projects (2014-Present)*, Paper 483, City University of New York, 2014, http://academicworks.cuny.edu/gc_etds/483.
[26]F. Dolde, I. Jakobi, B. Naydenov, N. Zhao, S. Pezzagna, C. Trautmann, J. Meijer, P. Neumann, F. Jelezko, and J. Wrachtrup, Nat. Phys. **9**, 139 (2013).
[27]L. Wang, J. Shi, Y. Zhu, Q. He, H. Xing, J. Zhou, F. Chen, and F. Chen, Langmuir **28**, 4920 (2012); V. R. Manfrinato, L. Zhang, D. Su, H. Duan, R. G. Hobbs, E. A. Stach, and K. K. Berggren, Nano Lett. **13**, 1555 (2013).
[28]M. S. Mastuli, N. Kamarulzaman, M. A. Nawawi, A. M. Mahat, R. Rusdi, and N. Kamarudin, Nanoscale Res. Lett. **9**, 134 (2014).
[29]N. Sutradhar, A. Sinhamahapatra, S. K. Pahari, P. Pal, H. C. Bajaj, I. Mukhopadhyay, and A. B. Panda, J. Phys. Chem. C **115**, 12308 (2011).